The Effects of Aeroelastic Tailoring on Flight Dynamic Stability

Natella, Mario; Wang, Xuerui; De Breuker, Roeland

DOI
10.2514/6.2018-0191

Publication date
2018

Document Version
Final published version

Published in
2018 AIAA/ASCE/AHS/ASC Structures, Structural Dynamics, and Materials Conference

AIAA SciTech Forum
8–12 January 2018, Kissimmee, Florida
2018 AIAA/ASCE/AHS/ASC Structures, Structural Dynamics, and Materials Conference

10.2514/6.2018-0191

The Effects of Aeroelastic Tailoring on Flight Dynamic Stability

Mario Natella*, Xuerui Wang†, and Roeland De Breuker‡
Delft University of Technology, Delft, Zuid-Holland, 2629HS, The Netherlands

This paper presents a unified framework for aeroelastic tailoring of free-flying aircraft with composite wings. A continuous-time state-space model is used to describe the flow. The 3D composite wing structures is condensed into a Timoshenko beam model by means of a cross-sectional modeler. The aerodynamic and structural models are closely coupled with the six degrees of freedom flight dynamic equations of motion in the state-space formulation. This paper refers to the clamped-wing aeroelastic tailoring as *classic aeroelastic tailoring*. Hence, the term *aeroelastic tailoring* will point at the novel approach that includes free-flying aeroelastic phenomena into the optimization process. The emphasis of the present paper is to show the effects of aeroelastic tailoring on body-freedom flutter and flight dynamic stability at large. The results of this paper will be used in the further development of aeroelastic tailoring practices for composite aircraft design.

I. Introduction

The period between 1980-1990 saw a unprecedented development in wing structural design practices due to the use of composite materials. The physical understanding of the properties of composite materials grew stronger and stronger in those years thus providing engineers and designers with new viable and innovative solutions. One of the solutions made possible because of composite materials is *classic aeroelastic tailoring*. As defined by M. Shirk et al.[1] in 1987, classic aeroelastic tailoring is the *embodyment of directional stiffness in aircraft design, to enhance its performance*.
Proving this concept on the scale of commercial aircraft is an ongoing challenge in this field of research. The *classic aeroelastic tailoring* optimization methods have already been proven very promising in latest developments on composite wing design. Among the benefits of aeroelastic tailoring, we find *(i)* weight reduction, *(ii)* root-bending moment alleviation and *(iii)* optimized distribution of properties and material throughout the structure. The degree of said effects is highly dependent on the load cases selected for the optimization. A study from T. Weisshaar et al.[2] in 1957 was one of the first studies to show the benefits of such a practice in structural design. Weisshaar et al. show how *classic aeroelastic tailoring* leads to the design of structures at maximized flutter speed (intended as clamped-root flutter). In his work it has also been mentioned that while the flutter speed was being maximized, *classic aeroelastic tailoring* contributes to minimizing the body-freedom flutter speed. This is a dynamic instability that involves aircraft pitch and plunge in combination with wing deformations. Said dynamic instability is more critical for flexible aircraft configurations.

The motivation behind this work is the need for a unified framework for analysis and optimization of modern composite aircraft. The integrated approach, combining aeroelasticity, flight dynamics and aeroelastic tailoring practices, is a natural evolution of engineering design given the challenges ahead of us. The theoretical framework has been throughly investigated in literature, showing the importance of flight dynamics in aeroelastic analyses. Some representative contributions are made by Cesnik[10], Patil[11, 12], Meirovitch[13] and Palacios[14].

*PhD Candidate, Department of Aerospace Structures and Materials, Delft University of Technology. M.Natella@tudelft.nl.
†PhD Candidate, Department of Control and Operations, Delft University of Technology. X.Wang-6@tudelft.nl.
‡Associate Professor, Department of Aerospace Structures and Materials, Delft University of Technology. R.DeBreuker@tudelft.nl.

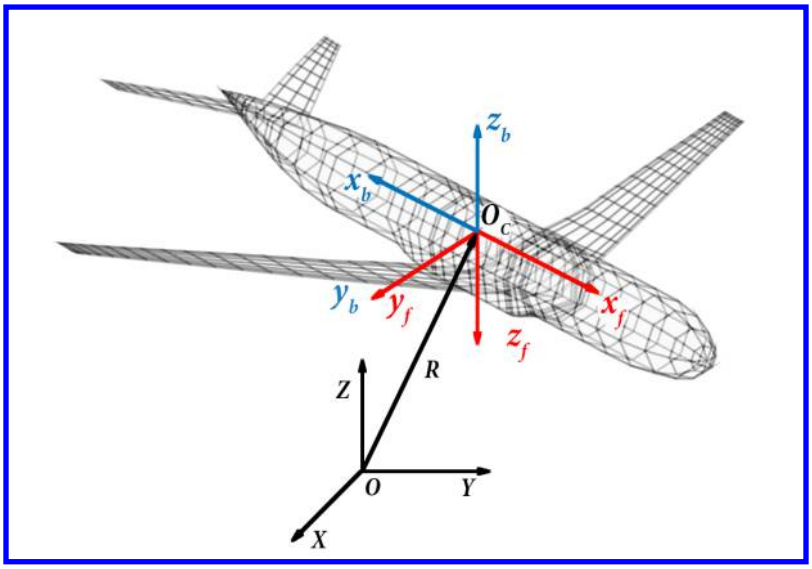

Fig. 1 Frame definitions.

The purpose of this study is twofold. On one hand, to present a unified aeroelastic framework for free-flying aircraft that is suitable for integrated aeroelastic stability analyses, aeroelastic tailoring practices and active control law design. On the other hand, to discuss the evolution of flight dynamic stability in a *classic* aeroelastic tailoring optimization. The framework developed within the scope of this paper is applied on the NASA Common Research Model (CRM) model*. The structure has been designed using composite materials and in such a way that a desirable degree of flexibility was reached. This model has a nonlinear static aeroelastic trim solution, so its stability is assessed linearizing around the nonlinear trim solution. Flutter, phugoid and short period modes are monitored throughout the optimization.

II. Model Descriptions

A. Rigid-Body Flight Dynamics

The nonlinear six degrees of freedom (6DoF) rigid-body dynamic equations of motion (EOM) in the body-fixed flight dynamic frame (O_c, x_f, y_f, z_f) can be written as (Etkin [15]),

$$\begin{aligned} m\dot{\mathbf{V}} &= -m\boldsymbol{\omega} \times \mathbf{V} + \mathbf{F} \\ \mathbf{J}\dot{\boldsymbol{\omega}} &= -\boldsymbol{\omega} \times \mathbf{J}\boldsymbol{\omega} + \mathbf{M} \\ \dot{\boldsymbol{\theta}} &= \mathbf{E}_f^{-1}\boldsymbol{\omega} \\ \dot{\mathbf{R}} &= \mathbf{C}_f^T\mathbf{V} \end{aligned} \tag{1}$$

The body-fixed flight dynamic frame (O_c, x_f, y_f, z_f) has its origin on the aircraft center of gravity (c.g.) and with $O_c x_f z_f$ represents the aircraft symmetrical plane as illustrated in Fig. 1. Conventionally, the aeroelastic solutions are calculated in the body-fixed frame (O_c, x_b, y_b, z_b), which has opposite $O_c x_b$ and $O_c z_b$ directions compared to the (O_c, x_f, y_f, z_f) frame.

In Eq. 1, $\mathbf{V}$ and $\boldsymbol{\omega}$ represent the translation and rotational velocities of the (O_c, x_f, y_f, z_f) frame relative to the inertial frame (O, X, Y, Z). $\mathbf{R}$ and $\boldsymbol{\theta}$ indicate the position and Euler angles of the (O_c, x_f, y_f, z_f) frame relative to (O, X, Y, Z). m is the total mass and $\mathbf{J}$ represents the inertia matrix. $\mathbf{F}$ and $\mathbf{M}$ are the total force and moment vectors. $C_f(\phi, \theta, \psi)$ is the rotation transformation matrix from inertial axes (O, X, Y, Z) to (O_c, x_f, y_f, z_f), and the $E(\phi, \theta)$ matrix links angular velocities $\boldsymbol{\omega}$ to Eulerian velocities $\dot{\boldsymbol{\theta}}$. Bold mark

*https://commonresearchmodel.larc.nasa.gov

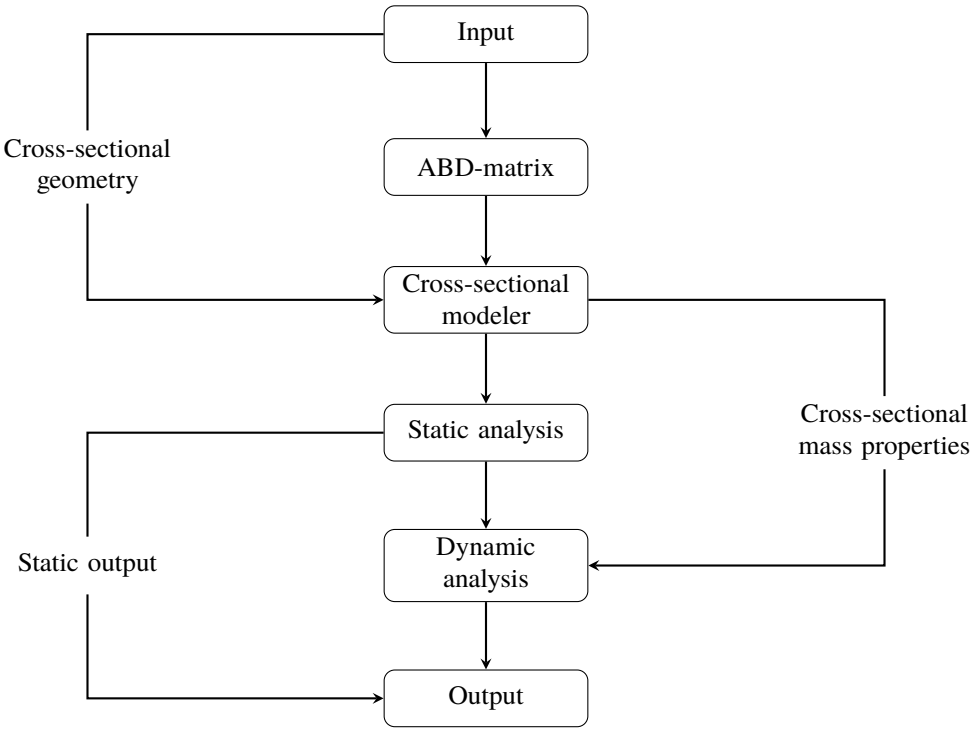

Fig. 2 Structural analysis flow chart, Werter et al. [7].

indicates vectors and matrices.

In this paper, gravity is modeled as a concentrated force acting on the c.g., which means the gravity has no contribution to the aeroelastic stiffness. The total force in Eq. 1 can be written as the summation of aerodynamic and gravitational forces as $\mathbf{F} = \mathbf{F}_a + \mathbf{F}_g$. When expressed in the flight dynamic frame, $\mathbf{F}_g = C_f[0,\ 0,\ mg]^T$, in which g represents the gravitational acceleration.

Under small perturbations, Eq. 1 can be linearized around an equilibrium point and expressed in the state-space form. Define the rigid-body states as $\mathbf{X}_f = [\Delta\mathbf{V},\ \Delta\boldsymbol{\omega},\ \Delta\mathbf{R},\ \Delta\boldsymbol{\theta}]^T$, where Δ indicate the variations with respect to the equilibrium condition. The linearized rigid-body dynamic equations can be expressed by

$$\dot{\mathbf{X}}_f = \mathbf{A}_{\mathrm{rr}}\mathbf{X}_f + \begin{bmatrix} \mathbf{M}_f^{-1} \\ \hline \mathbf{0} \end{bmatrix} \mathbf{F}_f \tag{2}$$

where $\mathbf{F}_f = [\Delta\mathbf{F}_a,\ \Delta\mathbf{M}_a]^T$ indicates the variations of the aerodynamic forces and moments with respect to the equilibrium point. $\mathbf{M}_f = \mathrm{diag}([m\mathbf{I}_3,\ \mathbf{J}])$ represents the flight dynamic mass matrix. Since $\mathbf{F}_g$ is a function of the Euler angles, it can be incorporated into the $\mathbf{A}_{\mathrm{rr}}$ matrix.

B. Structural Dynamics

The wing structure is modeled with Timoshenko beam elements described in a corotational frame of reference (FoR), Werter et al. [7]. The corotational frame is rigidly connected to the element and moves with the deformation of the beam at the particular point. A detailed mathematical derivation of the structural system in a corotational framework is presented in the the work of Battini and Pacoste [4]. The main advantage presented by the corotational approach is that the rigid connection renders the direction of the aerodynamic element constant irregardless of the local deformation.

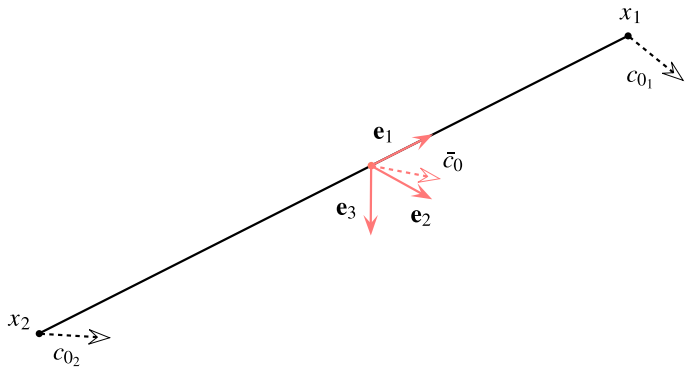

Fig. 3 Linear cross-sectional element of the wing FE model.

A logical chart of the structural analysis is shown in Fig. 2. The analysis commences with the modeling of the structural properties, described in terms of lamination parameters. Said parameters are then translated in cross-sectional properties assigned to a particular node locations. The formulation as such is suitable for both analysis and optimization of composite wing structures. Customary in optimization of composite structure is to opt for a discrete formulation of the problem, given the discrete nature of the thickness of a composite laminate. However, the introduction of lamination parameter allows for a continuous formulation of the optimization problem yielding to a convex design space wherein lies the optimum, Setoodeh et al.[3]

The stiffness matrices derived from the classical lamination theory can be writtern as a function of 15 lamination parameters and the material invariants, Gürdal et al.[5]. The aeroelastic framework assumes symmetric laminate, thus reducing the lamination parameters to 10 for a thorough description of the laminate. From this assumption also follows the de-coupling between in-plane and out-of-plane deformations, and prevention of out-of-plane warping.
Unbalanced laminate are allowed, thus accounting for the bending-torsion coupling in composite laminates, a key-stone in aeroelastic tailoring optimization.

Once the laminate has been properly described, the cross-sectional properties are to be translated in equivalent properties to lump in a specific node of the wing FE model. The computation of the equivalent properties is performed by means of the cross-sectional modeler, see Fig. 2, developed by Willaert et al.[6]. The formulation as such evaluates the Timoshenko stiffness matrix of a thin-walled cross-section, discretized in N elements. Material properties and thickness are assumed constant within an element, although changes between elements are allowed. From the Timoshenko stiffness matrix, the static response of the wing is thus determined. The dynamic analysis, linear about the nonlinear static equilibrium point, is then performed. For the analytical details refer to Werter et al.[7].

Brief Overview of the FE Model
The beam is modeled with N nodes, and $N-1$ elements, depending on the input specified in the input file. The length of the element is then evaluated. The number of mesh points of each section is determined by rounding up the length of the element divided by the average element length. The beam orientation is determined by the unit vectors $\mathbf{e}_1$, $\mathbf{e}_2$ and $\mathbf{e}_3$. The unit vector $\mathbf{e}_1$ is defined along the beam as shown in Fig. 3,

$$\mathbf{e}_1 = \frac{\mathbf{x}_2 - \mathbf{x}_1}{|\mathbf{x}_2 - \mathbf{x}_1|} \tag{3}$$

with 1 and 2 being the two end nodes of the beam element. The unit vector $\mathbf{e}_3$ is defined using $\mathbf{e}_1$ and the average chord direction $\mathbf{c}_{\text{avg}}$. Note that the average chord direction is the average of the chord directions at the end nodes. Having said that, unit vector $\mathbf{e}_3$ is given by,

$$\mathbf{e}_3 = \frac{\mathbf{e}_1 \times \mathbf{c}_{\text{avg}}}{|\mathbf{e}_1 \times \mathbf{c}_{\text{avg}}|} \tag{4}$$

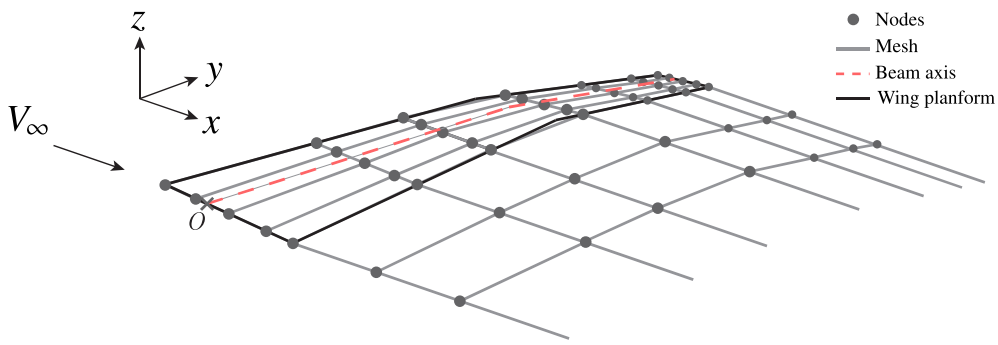

Fig. 4 Aerodynamic mesh in the aeroelastic framework developed by Wertel et al.[8].

The unit vector $\mathbf{e}_2$ is derived from $\mathbf{e}_1$ and $\mathbf{e}_3$ as follows,

$$\mathbf{e}_2 = \frac{\mathbf{e}_3 \times \mathbf{e}_1}{|\mathbf{e}_3 \times \mathbf{e}_1|} \tag{5}$$

For each structural elements thus generated, the local stiffness matrix is determined. The global matrix is then assembled using the co-rotational framework as developed and discussed in the work of Battini and Pacoste[4].

C. Aerodynamic Model

The aerodynamic module used in this work is the unsteady vortex-lattice method. The model is based on the unsteady potential flow theory under the assumption of incompressible, inviscid and irrotational flow, Werter et al.[8]. The governing equations can thus be written as,

$$\nabla^2 \Phi = 0 \tag{6}$$

subject to flow tangency (Eq. 7) and far-field boundary conditions (Eq. 8),

$$(\nabla \Phi + \mathbf{v}_\infty) \cdot \mathbf{n} = 0 \tag{7}$$

$$\lim_{d \to \infty} \nabla \Phi = 0 \tag{8}$$

For a unique solution of the aerodynamic problem, the wake has to be taken into account making sure that the Kutta condition is satisfied at the trailing edge, see Fig. 4 for a visual representation of the wake in the current aeroelastic framework. This means that the vortex strength has to be zero at the trailing edge. For the sake of completion, the shed vorticity can also be calculated remembering that the circulation $\mathbf{\Gamma}$ is zero around a curve enclosing the wing as proven by the Kelvin's theorem.

Omitting the extensive analytical derivation, that can be found in the work of [8], from the unsteady flow theory the following set of equations in state space formulation is obtained as follows,

$$\begin{bmatrix} \dot{\mathbf{\Gamma}} \\ \dot{\boldsymbol{\alpha}} \end{bmatrix} = \begin{bmatrix} \mathbf{K}_8 & \mathbf{K}_9 \\ \mathbf{0} & \mathbf{0} \end{bmatrix} \begin{bmatrix} \mathbf{\Gamma} \\ \boldsymbol{\alpha}' \end{bmatrix} + \begin{bmatrix} \mathbf{0} \\ \mathbf{I} \end{bmatrix} \dot{\boldsymbol{\alpha}}_{\text{inp}} \tag{9}$$

where $\boldsymbol{\alpha}'$ signifies the total angle of attack which includes the trim $\boldsymbol{\alpha}$ and the contributions of both structural and rigid states. The explicit expression for $\boldsymbol{\alpha}'$ will be derived in Chap. III.
What important for the aeroelastic coupling is the aerodynamic output in terms of forces and moments acting on the wing. The outputs are then to be lumped to the beam location at the particular section. Without going

into details of the analytical formulation, extensively illustrated in the work of Werter et al.[8], the output equation can be written as follows,

$$\begin{bmatrix} \mathbf{f}_a \\ \mathbf{m}_a \end{bmatrix} = \begin{bmatrix} \mathbf{L}_8 & \mathbf{L}_9 \end{bmatrix} \begin{bmatrix} \boldsymbol{\Gamma} \\ \boldsymbol{\alpha}' \end{bmatrix} + \mathbf{L}_7 \dot{\boldsymbol{\alpha}}' \tag{10}$$

It is important to notice that $\dot{\boldsymbol{\alpha}}'$ only affects the aerodynamic forces and not the vorticity $\boldsymbol{\Gamma}$.

III. Integrated Framework

In this section the state-space model that integrates aerodynamics and free-flying structural dynamics is derived. The derivation is carried out in two steps, first connecting the free-flying structural output to the aerodynamics input (Section A), then the aerodynamic output to the free-flying structural input (Section B).

A. From Aerodynamic Input to Structural Output

The aerodynamics in continuous-time state-space model is formulated in such a way that $\dot{\boldsymbol{\alpha}}$ is the input of the system. This model works under the assumption that the vertical gust (or excitation) is much smaller than V_∞. In the most general case, the angle of attack is a non-linear function of both the structural ($\mathbf{X}_s$) and the flight dynamic ($\mathbf{X}_f$) degrees of freedom,

$$\boldsymbol{\alpha}' = \boldsymbol{f}\left(\mathbf{X}_s, \mathbf{X}_f\right) \tag{11}$$

Linearizing the relationship we obtain the following expression for $\boldsymbol{\alpha}'$,

$$\boldsymbol{\alpha}' \approx \boldsymbol{\alpha} + \boldsymbol{\Theta} + \frac{\Delta \boldsymbol{x}_{\text{ea}}}{\mathrm{V}_\infty}\dot{\boldsymbol{\theta}}_s + \frac{\Delta \boldsymbol{x}_{\text{cg}}}{\mathrm{V}_\infty} q - \frac{\dot{\boldsymbol{h}}_s}{\mathrm{V}_\infty} + \frac{\dot{h}_r}{\mathrm{V}_\infty} \tag{12}$$

where $\boldsymbol{\Theta}$ is the angle of attack increment caused by the combined flexible and rigid rotations, $\dot{\boldsymbol{\theta}}_s$ refers to the structural angular velocity, q to the rigid angular velocity, $\Delta \boldsymbol{x}_{\text{ea}}$ and $\Delta \boldsymbol{x}_{\text{cg}}$ are the distances with respect to the elastic axis and center of gravity respectively, $\dot{\boldsymbol{h}}_s$ and $\dot{h}_r$ are the flexible and rigid plunge velocity respectively. Note that q and $\dot{h}_r$ are not vectors since they are identical for every element.

In a linearized model, the angle of attack can be re-written as a function of the structural and flight dynamic states, referred to as $\mathbf{X}_s$ and $\mathbf{X}_f$ and defined as,

$$\mathbf{X}_s^T = \Delta\left[\boldsymbol{\delta}_{s,1} \;\; \boldsymbol{\theta}_{s,1} \;\; \ldots \;\; \boldsymbol{\delta}_{s,i} \;\; \boldsymbol{\theta}_{s,i} \;\; \ldots \;\; \boldsymbol{\delta}_{s,N} \;\; \boldsymbol{\theta}_{s,N}\right] \tag{13}$$

$$\mathbf{X}_f^T = \left[\Delta \mathbf{V} \;\; \Delta \boldsymbol{\omega} \;\; \Delta \mathbf{R} \;\; \Delta \boldsymbol{\theta}\right] \tag{14}$$

where,

$$\boldsymbol{\delta}_{s,i}^T = \left[\delta_{x,i} \;\; \delta_{y,i} \;\; \delta_{z,i}\right] \tag{15}$$

$$\boldsymbol{\theta}_{s,i}^T = \left[\theta_{x,i} \;\; \theta_{y,i} \;\; \theta_{z,i}\right] \tag{16}$$

with $i = 1, \;\cdots,\; N$, where N is the number of structural elements. The linear expression for the angle of attack thus becomes,

$$\boldsymbol{\alpha}' = \left[\begin{array}{c|c|c} \mathbf{0} \quad \mathbf{I} & \boldsymbol{\Psi}_1 & \boldsymbol{\Psi}_2 \end{array}\right] \left[\begin{array}{c} \boldsymbol{\Gamma} \\ \boldsymbol{\alpha} \\ \hline \dot{\mathbf{X}}_s \\ \mathbf{X}_s \\ \hline \mathbf{X}_f \end{array}\right] \tag{17}$$

where $\boldsymbol{\Psi}_i$, with $i = 1, 2$, is nothing other than a selection matrix which translates the states into their respective influence on the angle of attack.

By using the linear expression for the angle of attack in Eq. 9, we have,

$$\begin{bmatrix} \dot{\mathbf{\Gamma}} \\ \dot{\boldsymbol{\alpha}} \end{bmatrix} = \begin{bmatrix} \mathbf{K}_8 & \mathbf{K}_9 & \mathbf{K}_9\mathbf{\Psi}_1 & \mathbf{K}_9\mathbf{\Psi}_2 \\ \mathbf{0} & \mathbf{0} & \mathbf{0} & \mathbf{0} \end{bmatrix} \mathbf{X} + \begin{bmatrix} \mathbf{0} \\ \mathbf{I} \end{bmatrix} \dot{\boldsymbol{\alpha}}_{\text{inp}} \tag{18}$$

where $\mathbf{X} = \left[\mathbf{\Gamma}^{\mathrm{T}}, \boldsymbol{\alpha}^{\mathrm{T}}, \dot{\mathbf{X}}_s^{\mathrm{T}}, \mathbf{X}_s^{\mathrm{T}}, \mathbf{X}_f^{\mathrm{T}}\right]^{\mathrm{T}}$, which for convenience we can re-write as,

$$\begin{bmatrix} \dot{\mathbf{\Gamma}} \\ \dot{\boldsymbol{\alpha}} \end{bmatrix} = \mathbf{H}_1\mathbf{T}_1\mathbf{X} + \mathbf{H}_7\dot{\boldsymbol{\alpha}}_{\text{inp}} \tag{19}$$

with $\mathbf{T}_1$ being a boolean selection matrix to select the appropriate contributions to the angle of attack.

Similarly, from Eq. 9 and 10, the aerodynamic force can be written as,

$$\begin{bmatrix} \mathbf{f}_a \\ \mathbf{m}_a \end{bmatrix} = \begin{bmatrix} \mathbf{L}_8 & \mathbf{L}_9 & \mathbf{L}_9\mathbf{\Psi}_1 & \mathbf{L}_9\mathbf{\Psi}_2 \end{bmatrix} \mathbf{X} + \begin{bmatrix} \mathbf{0} & \mathbf{0} & \mathbf{L}_7\mathbf{\Psi}_1 & \mathbf{L}_7\mathbf{\Psi}_2 \end{bmatrix} \dot{\mathbf{X}} + \mathbf{L}_7\dot{\boldsymbol{\alpha}}_{\text{inp}} \tag{20}$$

or equivalently,

$$\begin{bmatrix} \mathbf{f}_a \\ \mathbf{m}_a \end{bmatrix} = \mathbf{H}_2\mathbf{T}_1\mathbf{X} + \mathbf{H}_3\mathbf{T}_2\dot{\mathbf{X}} + \mathbf{L}_7\dot{\boldsymbol{\alpha}}_{\text{inp}} \tag{21}$$

with $\mathbf{T}_2$ being a boolean selection matrix for the contributions to the input $\dot{\boldsymbol{\alpha}}$.

B. From Aerodynamic Output to Structural Input

In this section, the distributed aerodynamic forces $\mathbf{f}_a$ and moments $\mathbf{m}_a$ acting on panels are transformed into concentrated aerodynamic forces $\mathbf{F}_a$ and moment $\mathbf{M}_a$ in the flight dynamic equations, as well as the elastic forces $\mathbf{f}_s$ acting on the structural nodes.

The total force $\mathbf{F}_a$ and moment $\mathbf{M}_a$ are simply summations of $\mathbf{f}_a$ and $\mathbf{m}_a$ respectively, and can be written in the matrix form as $\mathbf{F}_f = [\Delta\mathbf{F}_a, \Delta\mathbf{M}_a]^T = \mathbf{H}_{FA}[\mathbf{f}_a,\ \mathbf{m}_a]^T$, where $\mathbf{H}_{FA}$ is a Boolean matrix.
The transformation from $\mathbf{f}_a$ to $\mathbf{f}_s$ is based on the nearest neighbor method, which means the distributed aerodynamic force on each panel is inflicted by the nearest structure node. A Boolean matrix can be created by placing 1 for the selected panel location. This interpolation can be expressed by $\mathbf{f}_s = \mathbf{H}_{SA}[\mathbf{f}_a,\ \mathbf{m}_a]^T$.

Using Eq. 2, the EOM of the flexible-body dynamics can be given in its general form as,

$$\left[\begin{array}{c} \ddot{\mathbf{X}}_s \\ \dot{\mathbf{X}}_s \\ \hline \dot{\mathbf{X}}_f \end{array}\right] = \mathbf{A}_s \left[\begin{array}{c} \dot{\mathbf{X}}_s \\ \mathbf{X}_s \\ \hline \mathbf{X}_f \end{array}\right] + \left[\begin{array}{cc} \mathbf{M}_s^{-1} & \mathbf{0} \\ \mathbf{0} & \mathbf{0} \\ \hline \mathbf{0} & \mathbf{M}_f^{-1} \\ \mathbf{0} & \mathbf{0} \end{array}\right] \begin{bmatrix} \mathbf{f}_s \\ \mathbf{F}_f \end{bmatrix} \tag{22}$$

where $\mathbf{M}_s, \mathbf{C}_s, \mathbf{K}_s$ respectively represent the structural mass, damping and stiffness matrices. Applying the force transformation, we have,

$$\left[\begin{array}{c} \ddot{\mathbf{X}}_s \\ \dot{\mathbf{X}}_s \\ \hline \dot{\mathbf{X}}_f \end{array}\right] = \mathbf{A}_s \left[\begin{array}{c} \dot{\mathbf{X}}_s \\ \mathbf{X}_s \\ \hline \mathbf{X}_f \end{array}\right] + \left[\begin{array}{c} \mathbf{M}_s^{-1}\mathbf{H}_{SA} \\ \mathbf{0} \\ \hline \mathbf{M}_f^{-1}\mathbf{H}_{FA} \\ \mathbf{0} \end{array}\right] \begin{bmatrix} \mathbf{f}_a \\ \mathbf{m}_a \end{bmatrix} \tag{23}$$

By introducing a boolean selection matrix $\mathbf{T}_3$, such that,

$$\left[\begin{array}{c} \dot{\mathbf{X}}_s \\ \mathbf{X}_s \\ \hline \mathbf{X}_f \end{array}\right] = \mathbf{T}_3 \left[\begin{array}{c} \mathbf{\Gamma} \\ \boldsymbol{\alpha} \\ \hline \dot{\mathbf{X}}_s \\ \mathbf{X}_s \\ \hline \mathbf{X}_f \end{array}\right] \tag{24}$$

we can rewrite Eq. 23 as,

$$\begin{bmatrix} \ddot{\mathbf{X}}_s \\ \dot{\mathbf{X}}_s \\ \dot{\mathbf{X}}_f \end{bmatrix} = \mathbf{A}_s \mathbf{T}_3 \mathbf{X} + \mathbf{B}_s \begin{bmatrix} \mathbf{f}_a \\ \mathbf{m}_a \end{bmatrix} \tag{25}$$

C. State-Space Model

The state-space model is assembled by combining the flight dynamic, structural, aerodynamic models and the corresponding transfer functions defined previously in this paper.
Let us begin by substituting the force relationship (derived in Eq. 20) into Eq. 25 thus obtaining,

$$\begin{bmatrix} \ddot{\mathbf{X}}_s \\ \dot{\mathbf{X}}_s \\ \dot{\mathbf{X}}_f \end{bmatrix} = \mathbf{A}_s \mathbf{T}_3 \mathbf{X} + \mathbf{B}_s \left(\mathbf{H}_2 \mathbf{T}_1 \mathbf{X} + \mathbf{H}_3 \mathbf{T}_2 \dot{\mathbf{X}} + \mathbf{L}_7 \dot{\boldsymbol{\alpha}}_{\text{inp}} \right) \tag{26}$$

combining with Eq. 19,

$$\dot{\mathbf{X}} = \begin{bmatrix} \mathbf{0} \\ \mathbf{B}_s \mathbf{H}_3 \mathbf{T}_2 \end{bmatrix} \dot{\mathbf{X}} + \begin{bmatrix} \mathbf{H}_1 \mathbf{T}_1 \\ \mathbf{A}_s \mathbf{T}_3 + \mathbf{B}_s \mathbf{H}_2 \mathbf{T}_1 \end{bmatrix} \mathbf{X} + \begin{bmatrix} \mathbf{H}_7 \\ \mathbf{B}_s \mathbf{L}_7 \end{bmatrix} \dot{\boldsymbol{\alpha}}_{\text{inp}} \tag{27}$$

or equivalently,

$$\left(\mathbf{I} - \mathbf{H}_4 \right) \dot{\mathbf{X}} = \mathbf{H}_5 \mathbf{X} + \mathbf{H}_6 \dot{\boldsymbol{\alpha}}_{\text{inp}} \tag{28}$$

and finally,

$$\dot{\mathbf{X}} = \left(\mathbf{I} - \mathbf{H}_4 \right)^{-1} \mathbf{H}_5 \mathbf{X} + \left(\mathbf{I} - \mathbf{H}_4 \right)^{-1} \mathbf{H}_6 \dot{\boldsymbol{\alpha}}_{\text{inp}} \tag{29}$$

The coupled state matrix is shown in Eq. 30. The matrices $\mathbf{T}$ refer to off-diagonal coupling terms, with the subscripts A, S and F refer to aerodynamic, structural and flight dynamic states respectively. The $\mathbf{T}$ matrices can be calculated from Eq. 29. It can be proven that $\mathbf{T}_{\text{SF}} = \mathbf{T}_{\text{FS}} = \mathbf{0}$, which indicates the absence of inertia coupling between structural and flight dynamics via the presented approach. The influence of such inertial couplings will be analyzed in future work.

From this system we can easily derive other dynamic equations, namely aeroelasticity, flight dynamics, and free-flying flexible-body dynamics. The flight dynamic state-space equations are obtained by the combination of aerodynamic and rigid-body dynamics as shown in Eq. 31, also referred to as quasi-rigid aircraft.

$$\left[\begin{array}{c} \dot{\boldsymbol{\Gamma}} \\ \dot{\boldsymbol{\alpha}} \\ \hline \ddot{\mathbf{X}}_s \\ \dot{\mathbf{X}}_s \\ \hline \dot{\mathbf{X}}_f \end{array}\right] = \left[\begin{array}{cc:cc:c} \mathbf{K}_8 & \mathbf{K}_9 & \multicolumn{2}{c:}{\multirow{2}{*}{$\mathbf{T}_{\text{AS}}$}} & \multirow{2}{*}{$\mathbf{T}_{\text{AF}}$} \\ \mathbf{0} & \mathbf{0} & \multicolumn{2}{c:}{} & \\ \hdashline \multicolumn{2}{c:}{\multirow{2}{*}{$\mathbf{T}_{\text{SA}}$}} & $-\mathbf{M}_s^{-1}\mathbf{C}_s$ & $-\mathbf{M}_s^{-1}\mathbf{K}_s$ & \multirow{2}{*}{$\mathbf{T}_{\text{SF}}$} \\ \multicolumn{2}{c:}{} & $\mathbf{I}$ & $\mathbf{0}$ & \\ \hdashline \multicolumn{2}{c:}{$\mathbf{T}_{\text{FA}}$} & \multicolumn{2}{c:}{$\mathbf{T}_{\text{FS}}$} & $\mathbf{A}_{\text{rr}}$ \end{array}\right] \left[\begin{array}{c} \boldsymbol{\Gamma} \\ \boldsymbol{\alpha} \\ \hline \dot{\mathbf{X}}_s \\ \mathbf{X}_s \\ \hline \mathbf{X}_f \end{array}\right] + \mathbf{B}\dot{\boldsymbol{\alpha}}_{\text{inp}} \tag{30}$$

$$\left[\begin{array}{c} \dot{\boldsymbol{\Gamma}} \\ \dot{\boldsymbol{\alpha}} \\ \hline \dot{\mathbf{X}}_f \end{array}\right] = \left[\begin{array}{cc:cc:c} \mathbf{K}_8 & \mathbf{K}_9 & \multicolumn{2}{c:}{\multirow{2}{*}{$\mathbf{T}_{\text{AF}}$}} & \\ \mathbf{0} & \mathbf{0} & \multicolumn{2}{c:}{} & \\ \hdashline \multicolumn{4}{c:}{$\mathbf{T}_{\text{AF}}$} & $\mathbf{A}_{\text{rr}}$ \end{array}\right] \left[\begin{array}{c} \boldsymbol{\Gamma} \\ \boldsymbol{\alpha} \\ \hline \mathbf{X}_f \end{array}\right] + \mathbf{B}'\dot{\boldsymbol{\alpha}}_{\text{inp}} \tag{31}$$

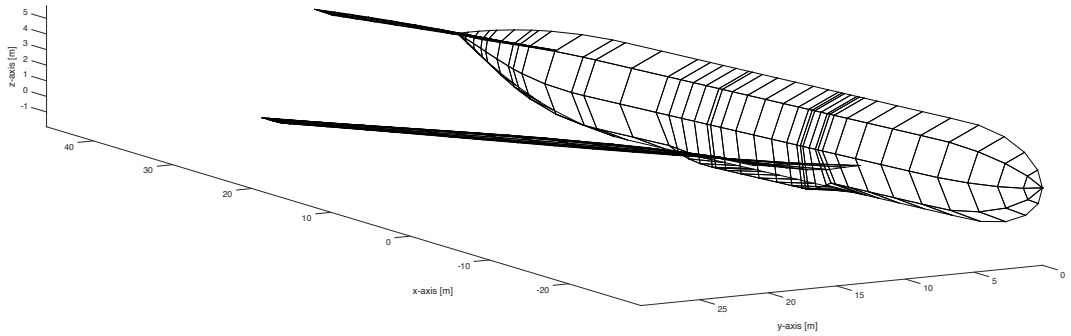

Fig. 5 Aerodynamic meshes of the NASA CRM aircraft.

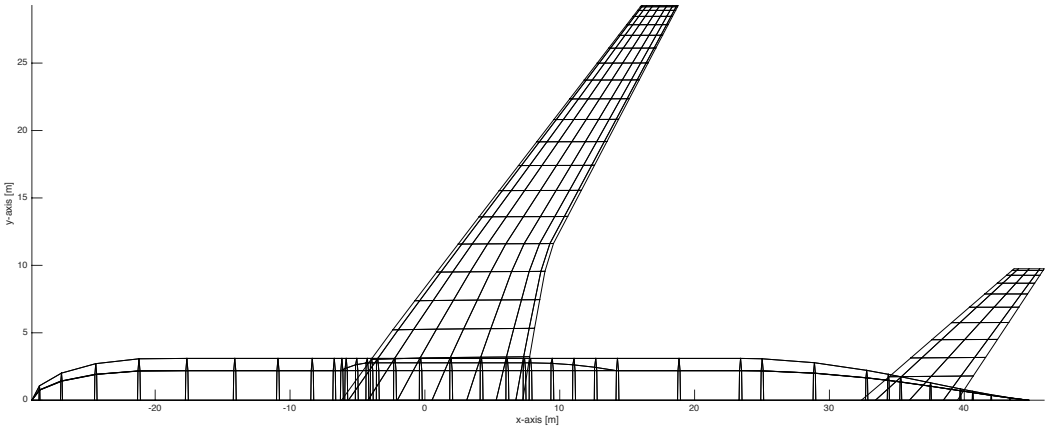

Fig. 6 Aerodynamic meshes of NASA CRM aircraft in top view.

IV. Stability Analyses on Benchmark Model

The model is based on NASA CRM aircraft model and falls within the CS25[†] category for conventional large commercial aircraft. A standard alloy (Aluminum 7075T73) has been used to model the material properties of the aircraft. The wing spans is 58.5 m, with a wetted surface of 410.7 m^2. The fuselage length is 73.9 m, with a diameter of approximately 6 m.

The aim of this section is to provide benchmark results for the free-flying aeroelastic aircraft, which will later be used for aeroelastic tailoring optimization. Reference values for flight dynamics responses have been taken from the CS25. Both the quasi-rigid and the fully-flexible aircraft model are analyzed and compared against the classic clamped aircraft responses.

A. Stability Analyses

The stability of the aircraft has been analyzed in cruise conditions at 136 m/s, at 11000 m altitude and Mach number of 0.85. The trim solution for this flight condition is at an angle of attack of 4.9°, and horizontal tail deflection of 2.8°.

[†]EASA Certifications on: https://www.easa.europa.eu/certification-specifications/cs-25-large-aeroplanes

Table 1 Modes of flexible aircraft clamped at the wing-root.
STR: structural modes, AE: aeroelastic modes.

	Frequency [Hz]	Damping Ratio [-]
I STR	2.02	-
II STR	5.47	-
III STR	7.77	-
IV STR	10.9	-
V STR	18.1	-
VI STR	19.2	-
VII STR	20.8	-
VIII STR	26.7	-
IX STR	31.4	-
X STR	35.9	-
I AE	0.874	-
II AE	1.19	0.180
III AE	1.39	0.838
IV AE	2.58	0.273
V AE	6.61	0.0708
VI AE	7.75	0.00205
VII AE	14.7	0.0325
VIII AE	20.6	0.000933
IX AE	25.2	0.0216
X AE	35.4	0.0128

Table 2 Modes of free-flying quasi-rigid aircraft.

	Frequency [Hz]	Damping Ratio [-]
Phugoid	0.0430	0.146
Short Period	1.28	0.781

The stability has been assessed for three different models, *(i)* the classic flexible aircraft model with clamped boundary conditions, Tab. 1, *(ii)* the free-flying quasi-rigid aircraft model, Tab. 2 and *(iii)* the free-flying flexible aircraft model, Tab. 3.

Table 3 Modes of free-flying flexible aircraft.
AE: aeroelastic modes.

	Frequency [Hz]	Damping Ratio [-]
Phugoid	0.0339	0.172
Short Period	1.38	0.913
I AE	1.05	-
II AE	1.38	0.913
III AE	1.47	0.206
IV AE	3.75	0.111
V AE	6.78	0.0604
VI AE	7.75	0.00243
VII AE	14.6	0.0391
VIII AE	20.5	0.000871
IX AE	25.2	0.0239
X AE	35.4	0.0128

Table 4 Material properties of CRM wing.[§]

Property	Value
E_{11}	$1.47 \cdot 10^{11}$
E_{22}	$1.03 \cdot 10^{10}$
G_{12}	$7.00 \cdot 10^{9}$
ν_{12}	0.27

V. Effects of Aeroelastic Tailoring on Free-Flying Stability

A. Optimization Set-up

The aeroelastic tailoring optimization has been set up for weight minimization. The CRM initial guess has been chosen to be stiff enough to be feasible and stable, with the following 0-dominated stacking sequence[‡],

$$[(0)_{60\%}, (90)_{10\%}, (\pm 45)_{30\%}]_s \tag{32}$$

The loads are calculated using a full-aircraft aerodynamic model. The fuselage and the horizontal tail are rigid, and not included in the tailoring process. They are only included in the calculation of the aircraft weight used for trim purposes. The wing is made of composite material with properties shown in Tab. 4.

The model is suject to the following constraints:

- feasibility of lamination paramenters, see Gürdal et al.[5],
- buckling failure index, see Dillinger et al.[9],
- strain failure index,
- aileron effectiveness,
- aeroelastic stability.

The flight dynamic stability is only monitored throughout the optimization, to observe its evolution. It is although not formulated as a constraint, thus allowing for the convergence to an design with unstable rigid body motions.

[‡]NB: the 0-direction refers to the direction that runs along the beam axis.
[§]SI units are used.

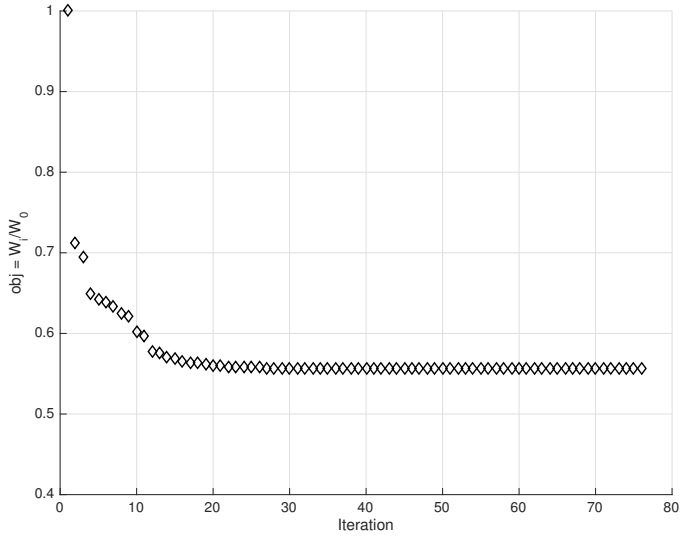

Fig. 7 Objective convergence.

B. Optimization Results and Observations

The phenomena observed as a result of the aeroelastic tailoring optimization are hereby discussed.

Optimized Stiffness and Mass Distribution

The objective converges to 0.55 as shown in Fig. 7. This normalized value corresponds to a mass of approximately 3800 kg. The optimized stiffness and thickness distribution is shown in Fig. 8. The skins and spars are thickened in the neighborhood of the engine location (approximately 10m in span-wise direction). The thickness is then further adjusted in case the section is under relatively high stresses.
The driver behind the stiffness optimization is twofold. The stiffness is tailored to *(i)* induce wash-out effect and *(ii)* control the buckling response. The latter has been found to be the main driver for the spar tailoring.

Modal Coalescence

As in classic aeroelasticity, modal coalescence is one of the mechanisms causing instabilities. Throughout the optimization we can observe how the 1^{st} aeroelastic mode and the phugoid reach a difference in frequency of only 0.1 Hz, as shown in Fig. 9. Aeroelastic stability has not been found critical for any of the design points.

Short Period Mode Instability

The short period mode has been found to be unstable during the optimization, as shown in Fig. 10. The physical explanation is hereby given. The objective of aeroelastic tailoring is weight minimization which implies a wing root bending moment minimization by moving lift inboard. For a swept-back wing, an inboard movement of the lift vector also implies a forward movement (towards the aircraft nose). At the same time, the center of gravity (c.g.) is also moving backward (towards the rear of the aircraft) due to the fact that the wing weight decreases during the optimization. These two factors cause the aerodynamic center (a.c.) moves in front of the c.g., which indicates an unstable short period mode.

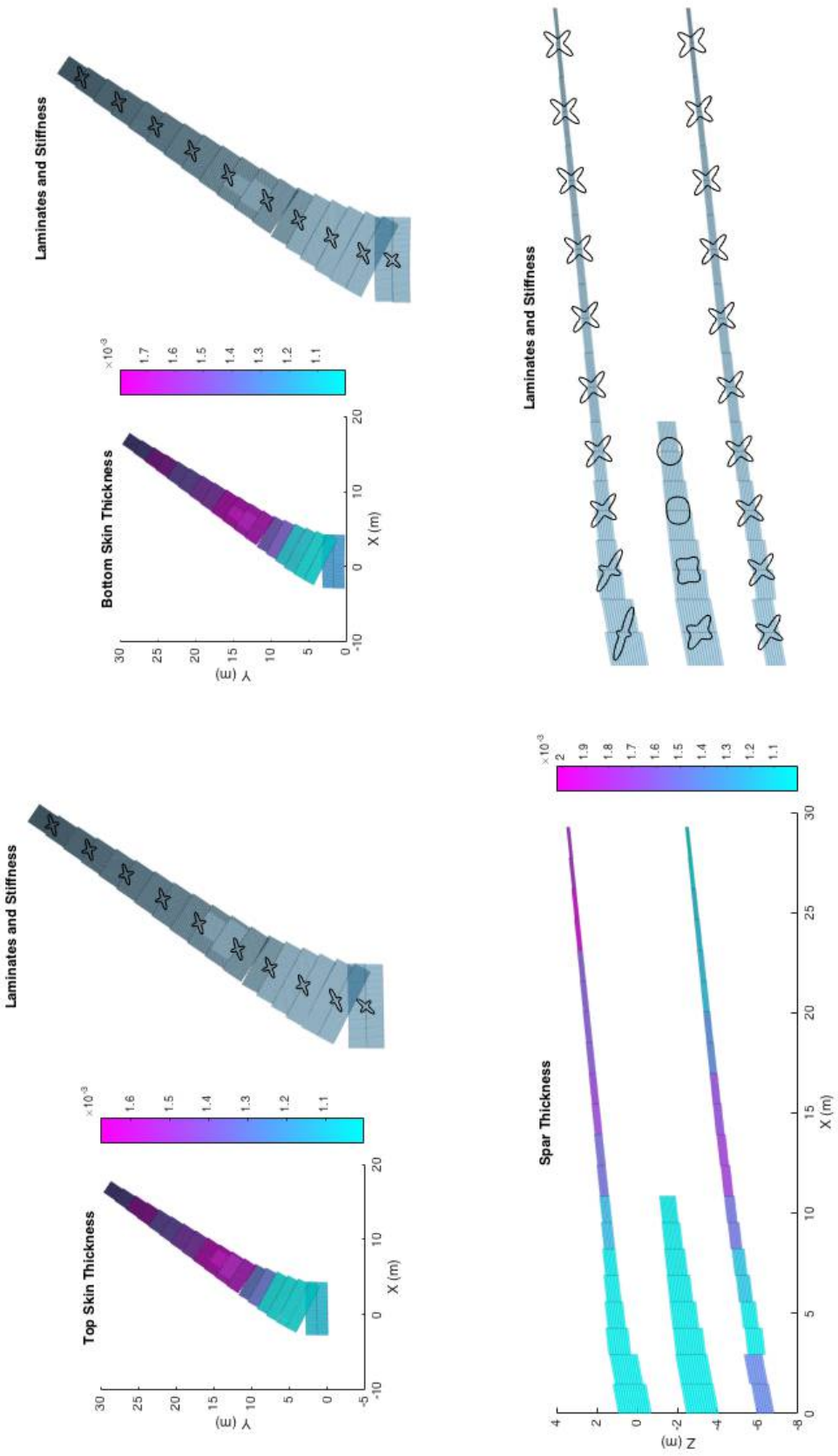

Fig. 8 Optimized stiffness and thickness distributions.

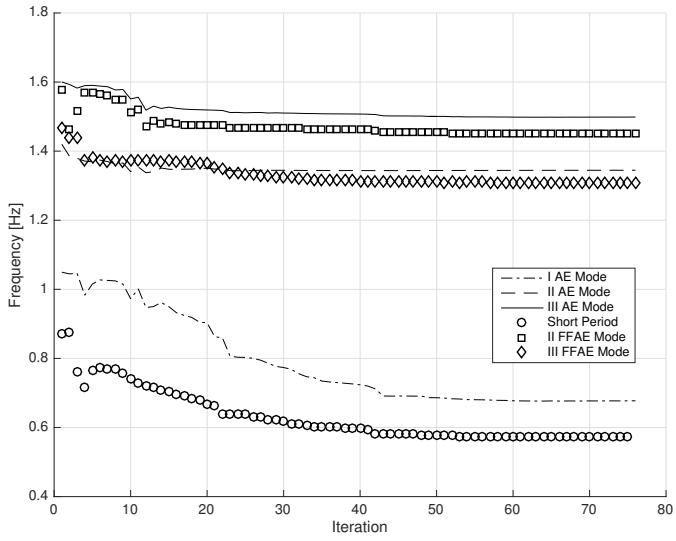

Fig. 9 History of modal frequencies during aeroelastic tailoring optimization.
AE : Aeroelastic, FFAE: Free-flying Aeroelasticity.

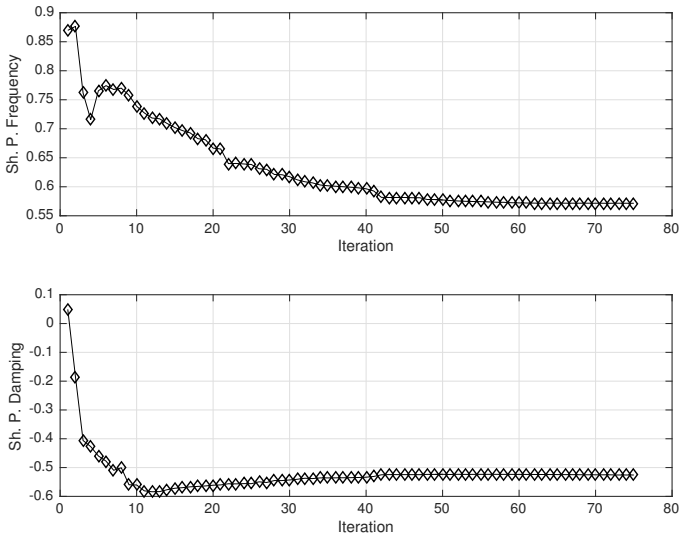

Fig. 10 History of short period frequency and damping during aeroelastic tailoring optimization.

VI. Conclusions and Recommendations

This work has shown the importance of flight dynamic stability for composite aircraft optimization. While the classic flutter speed, as in clamped-root flutter, is maximized, the body-freedom flutter speed is reduced, which makes the short period mode unstable in the tested flight condition.
The use of composite materials and the aeroelastic tailoring practices enhance the level of flexibility, also for conventional aircraft configuration, to a point where the body-freedom flutter becomes a critical phenomenon. This is not only important for stability but also for the aircraft maneuverability and handling qualities.

In future developments of this work, stability and handling quality constraints will be investigated. This will allow to perform aeroelastic tailoring optimization prescribing a certain level of maneuverability. This practice will be useful in designing new aircraft concepts and unconventional configurations via aeroelastic tailoring while guaranteeing desirable handling qualities.
An overall stability constraint for aeroelastic tailoring will also be formulated. An exception can be made for the slow and controllable rigid-body modes (e.g. phugoid, spiral modes) that can be easily controlled by the pilot in a large time scale. The three dimensional free-flying aeroelastic stability will also be investigated in the future research.

References

[1] Shirk, M.H., Hertz, T.J. and Weisshaar, T.A., “Aeroelastic Tailoring - Theory, Practice and Promise", *Journal of Aircraft*, Vol. 23, No. 1, 1987.

[2] Weisshaar, T.A., “Aeroelastic Tailoring - Creative Use of Unusual Materials", *AIAA/ASME/ASCE/AHS 28th Structures, Structural Dynamics and Material Conference*, Monterey, CA, AIAA 87-0976-CP, April 6-8 1987.

[3] Setoodeh, S., Abdalla, M., and Gurdal, Z., “Approximate feasible regions for lamination parameters”, 11th AIAA/ISSMO Multidisciplinary Analysis and Optimization Conference, 6-8 September 2006, Portsmouth, Virginia, USA.

[4] Battini, J.M., and Pacoste, C., “Co-rotational beam elements with warping effects in instability problems", *Computational Methods in Applied Mechanical Engineering*, 191, 2002, 1755-1789.

[5] Gurdal, Z., Haftka, R., and Hajela, P., “Design and optimization of laminated composite materials", *John Wiley and Sons*, Inc, 1999.

[6] Willaert, M., Abdalla, M., and Gurdal, Z., “A simple finite element cross-sectional modeling of thin-walled beams", *Proceedings of the 2nd Aicraft Structural Design Conference*, 2010.

[7] Werter, N., De Breuker, R., “A novel dynamic aeroelastic framework for aeroelastic tailoring and structural optimisation", *Composite Structures*, 2016, Vol. 158 - 369-386.

[8] Werter, N., De Breuker, R., and Abdalla, M., “Continuous-time stat-space unsteady aerodynamic modelling for efficient aeroelastic load analysis", *International Forum on Aeroelasticity and Structural Dynamics*, June 28 - July 2 2015, Saint Petersburg, Russia.

[9] Dillinger, J.K.S., “Static Aeroelastic Optimization of Composite Wings with Variable Stiffness Laminates". *PhD Dissertation*, Delft University of Technology, 2014.

[10] Shearer, C. M., Cesnik, C. E. S., “Nonlinear Flight Dynamics of Very Flexible Aircraft,” *Journal of Aircraft*, 2007, 44(5): 1528-1545.

[11] Patil, M. J., Hodges, D. H., “Flight Dynamics of Highly Flexible Flying Wings,” *Journal of Aircraft*, 2006, 43(6): 1790-1799.

[12] Patil, M. J., Hodges, D. H. S., Cesnik. C. E., “Nonlinear aeroelasticity and flight dynamics of high-altitude long-endurance aircraft,” *Journal of Aircraft*, 2001, 38(1): 88-94.

[13] Meirovitch, L., Tuzcu, I., “Unified Theory for the Dynamics and Control of Maneuvering Flexible Aircraft,” *AIAA Journal*, 2004, 42(4): 714-727.

[14] Palacios, R., Murua, J., Cook, R., “Structural and Aerodynamic Models in Nonlinear Flight Dynamics of Very Flexible Aircraft,” *AIAA journal*, 2010, 48(11): 2648-2659.

[15] Etkin, B., “Dynamics of Atmospheric Flight”, Dover Publications, Toronto, 2005.